Mononuclear and binuclear lanthanide(III) complexes: syntheses, structural, photophysical and thermal properties
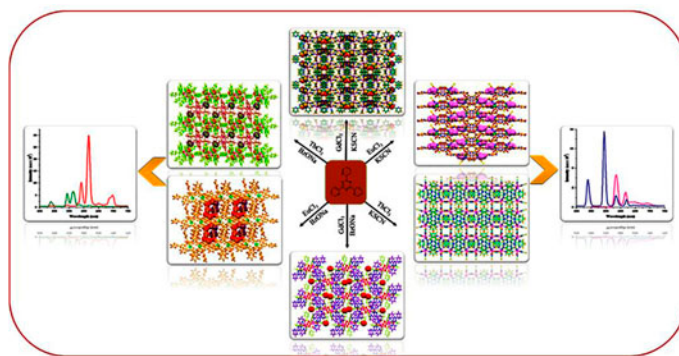
Nidhi Goel

Taylor & Francis
Taylor & Francis Group

Mononuclear and binuclear lanthanide(III) complexes: syntheses, structural, photophysical and thermal properties

NIDHI GOEL*

Department of Chemistry, Indian Institute of Technology Roorkee, Roorkee, India

Six new Ln(III) complexes viz., $[Gd(tptz)(SCN)_3(CH_3OH)_2OH_2]\cdot CH_3OH$ (**1**), $[Eu(tptz)(SCN)_3(CH_3OH)_2OH_2]\cdot CH_3OH$ (**2**), $[Tb(tptz)(SCN)_3(OH_2)_3]_4$ (**3**), $[Gd(tptz)(OBz)_2(\mu\text{-}OBz)OH]_2\cdot 2H_2O$ (**4**), $[OH_2(OBz)_2(tptz)Eu_1(\mu\text{-}OBz)_2Eu_2(tptz)(OBz)_2OH_2]\cdot CH_3OH\cdot 7H_2O$ (**5**), and $\{[Tb_1(tptz)(OBz)_2(\mu\text{-}OBz)]_2\cdot[Tb_2(tptz)(OBz)_3CH_3OH]_2\}\cdot 2CH_3OH\cdot 4H_2O$ (**6**) (Ln = Gd, Eu, Tb; tptz = 2,4,6-tris(2-pyridyl)-1,3,5-triazine; BzONa = sodium benzoate), have been synthesized and characterized by physicochemical methods including single-crystal X-ray crystallography. The X-ray studies demonstrate that **1–3** are mononuclear, whereas **4–6** are binuclear. The photophysical properties of **1–6** have been studied with ultraviolet absorption and emission spectral studies. Their thermal properties have been studied by thermogravimetric (TG) and derivative thermogravimetric analysis (DTG), demonstrating that the final product after decomposition was Ln_2O_3 for all these complexes.

Keywords: 2,4,6-Tris(2-pyridyl)-1,3,5-triazine; Sodium benzoate; X-ray study; Photophysical; Thermal property

1. Introduction

Because of photochemical properties and applications as function materials, lanthanide chemistry is of great interest [1–4]. Lanthanide ions have less tendency to absorb light, but complexes of lanthanide ions with organic ligands having N– and –COOH groups can

*Email: nidhigoel.iitr@gmail.com

absorb light strongly and show efficient luminescence as these organic ligands transfer intramolecular energy from excited ligand triplet states to the metal ion (antenna effect) [5–12]. According to molecular fragments principle, commonly used N-containing organic compounds act as the energy donors and luminescence sensitizers for lanthanide ions. An aromatic compound, 2,4,6-tris(2-pyridyl)-1,3,5-triazine (tptz), has been used as a multidentate ligand in coordination chemistry [13–17]. It is a tridentate ligand and decreases solvent-based vibrational coupling and luminescence quenching in most lanthanide complexes as it creates interference for coordination of the solvent [18]. The remaining nitrogens coordinate with other transition metals, and thus, tptz is involved in designing complicated heterometallic complexes, which have magnetic as well as luminescence properties [19–21]; tptz also acts as secondary ligand for some lanthanide complexes of carboxylates. Lanthanide carboxylate complexes show interesting crystal structures, high thermal and luminescent properties due to coordination versatility of these ligands. A large number of lanthanide complexes with N– and –COOH containing ligand have been studied [22–26], but photophysical, and thermal studies for Eu(III) and Tb(III) complexes with tptz and benzoate ligands are not reported. This paper describes the synthesis, structural, photophysical and thermal properties of some Ln(III) complexes. The main purpose is to see whether secondary ligands affect the structure and photophysical properties of some Ln(III) complexes, when compared with its mononuclear complexes.

2. Experimental

2.1. *Materials*

All manipulations were performed in air using commercial grade solvents. Potassium thiocyanate and benzoic acid were commercially available from S.D. Fine-Chem. Limited, whereas 2,4,6-tris(2-pyridyl)-1,3,5-triazine, $GdCl_3 \cdot 6H_2O$, $EuCl_3 \cdot 6H_2O$, and $TbCl_3 \cdot 6H_2O$ of the highest grade were purchased from Aldrich Chemical Company (USA) and used as received. Sodium benzoate was synthesized by the known procedure [27].

2.2. *Syntheses of complexes*

The general method for the syntheses of complexes is given in scheme 1.

2.2.1. Synthesis of [Gd(tptz)(SCN)$_3$(CH$_3$OH)$_2$OH$_2$]·CH$_3$OH (1). A mixture of potassium thiocyanate (0.15 g, 1.5 mM) and 2,4,6-tris(2-pyridyl)-1,3,5-triazine (0.15 g, 0.5 mM) in 15.0 ml methanol was added to methanolic solution of $GdCl_3 \cdot 6H_2O$ (0.19 g, 0.5 mM). The reaction mixture was stirred at room temperature for 8 h and the solution was filtered on Celite. The filtrate was dried under vacuum to afford a powder in 79.8% (0.60 g, 0.79 mM) yield. The compound was recrystallized from methanol at 4 °C. Anal. Calcd (%): C, 38.03; H, 3.45; N, 16.63; S, 12.69. Found: C, 37.81; H, 3.39; N, 16.15; S, 12.09. IR (KBr, cm^{-1}): 3443, 2067, 1630, 1545, 1519, 1381, 1256, 756, 627.

2.2.2. Synthesis of [Eu(tptz)(SCN)$_3$(CH$_3$OH)$_2$OH$_2$]·CH$_3$OH (2). Complex **2** was prepared and crystallized in 77.4% (0.58 g, 0.77 mM) yield by the same method as outlined
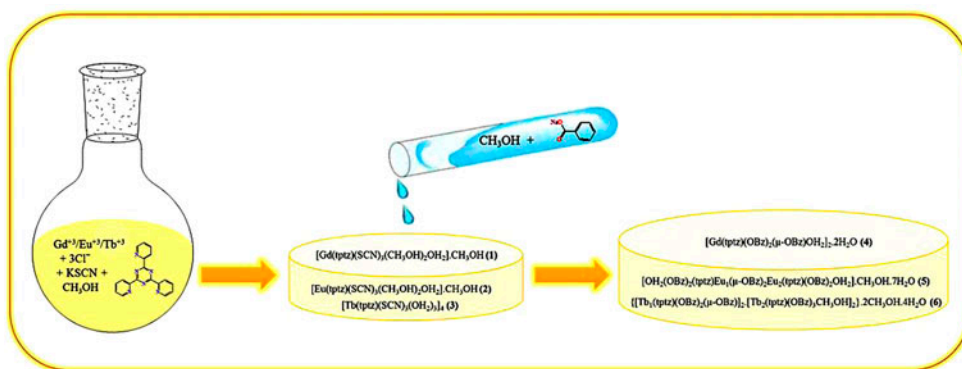
Scheme 1. General method for the synthesis of **1–6**.

for **1** using EuCl$_3$·6H$_2$O (0.18 g, 0.5 mM) instead of GdCl$_3$·6H$_2$O. Anal. Calcd (%): C, 38.29; H, 3.48; N, 16.74; S, 12.78. Found: C, 37.81; H, 3.39; N, 15.89; S, 12.03. IR (KBr, cm^{-1}): 3449, 2066, 1630, 1543, 1378, 1260, 1156, 1013, 763, 675.

2.2.3. Synthesis of [Tb(tptz)(SCN)$_3$(OH$_2$)$_3$]$_4$ (3). The same procedure was applied on **3** as outlined above for **1** using TbCl$_3$·6H$_2$O (0.19 g, 0.5 mM) with 74.9% (0.52 g, 0.75 mM) yield. Anal. Calcd (%): C, 36.05; H, 2.59; N, 18.02; S, 13.74. Found: C, 35.91; H, 2.57; N, 17.63; S, 13.11. IR (KBr, cm^{-1}): 3420, 2059, 1621, 1541, 1377, 1086, 763, 675.

2.2.4. Synthesis of [Gd(tptz)(OBz)$_2$(μ-OBz)OH$_2$]$_2$·2H$_2$O (4). A solution of sodium benzoate (0.21 g, 1.5 mM) in a water–methanol mixture (v/v %, 1 : 4, 10 ml) was added to solution of **1**, and the mixture was stirred at room temperature for 6 h. The solution was filtered on Celite, and the filtrate was dried under vacuum to afford a powder in 74.2% (1.3 g, 0.74 mM) yield. Anal. Calcd (%): C, 53.91; H, 3.36; N, 9.67. Found: C, 53.01; H, 3.28; N, 9.11. IR (KBr, cm^{-1}): 3425, 1612, 1599, 1537, 1421, 1017, 718, 676.

2.2.5. Synthesis of [OH$_2$(OBz)$_2$(tptz)Eu$_1$(μ-OBz)$_2$Eu$_2$(tptz)(OBz)$_2$OH$_2$]·CH$_3$OH·7H$_2$O (5). Complex **5** was also prepared by the same procedure as outlined above for **4** in 68.7% (1.27 g, 0.69 mM) yield. Anal. Calcd (%): C, 51.42; H, 3.93; N, 9.11. Found: C, 50.63; H, 3.89; N, 8.91. IR (KBr, cm^{-1}): 3445, 1614, 1599, 1541, 1421, 1021, 766, 718.

2.2.6. Synthesis of {[Tb$_1$(tptz)(OBz)$_2$(μ-Bz)]$_2$·[Tb$_2$(tptz)(OBz)$_3$CH$_3$OH]$_2$}·2CH$_3$OH·4H$_2$O (6). The same procedure was applied on **6** as outlined above for **4** in 73.7% (2.61 g, 0.74 mM) yield. Anal. Calcd (%): C, 54.31; H, 3.76; N, 9.50. Found: C, 53.77; H, 3.71; N, 8.67. IR (KBr, cm^{-1}): 3441, 1612, 1599, 1532, 1421, 1255, 1008, 854, 768, 722.

2.3. *Instrumentation*

Crystallized complexes were carefully dried under vacuum for several hours prior to elemental analysis on an Elementar Vario EL III analyzer. IR spectra were recorded on a

Thermo Nicolet Nexus FT-IR spectrometer on KBr pellets. Thermogravimetry and derivative thermogravimetry (TG–DTG) were carried out at 10 °C/min (mass 0.055 g) in air (flow rate of 200 ml min^{-1}) on a Perkin Elmer (Pyris Diamond) (Woodland, CA, USA) thermogravimetric analyzer.

2.4. Crystallographic study

Single-crystal X-ray diffraction data were collected at 100 K on a Bruker Kappa four circle-CCD diffractometer using graphite-monochromated Mo Kα radiation ($\lambda = 0.71070$ Å). Empirical absorption corrections were applied in reduction of data, Lorentz and polarization corrections [28]. The SHELXTL program was used for the structure solution, refinement, and data output [29, 30]. Nonhydrogen atoms were refined anisotropically, while hydrogens were placed in geometrically calculated positions by using a riding model. Images and hydrogen bonding interactions were created with DIAMOND and MERCURY software [31, 32]. Crystallographic data and selected hydrogen bond distances are given in tables 1 and 2, respectively.

3. Results and discussion

3.1. Infrared spectra

IR spectra of all the complexes show strong bands at 3545–3320 cm^{-1} due to v(OH) stretches of lattice and/or coordinated water [33]. In **1–3**, the presence of v(C–N) at 2067 cm^{-1} shows coordination of thiocyanate through the nitrogen. The C–N stretching frequencies of thiocyanates are generally lower in the N-bonded complexes than the S-bonded complexes (near 2010 cm^{-1}) [34]. The infrared spectra of **1–6** gave a strong absorption as an asymmetric doublet at 1551–1522 cm^{-1} due to stretching vibrations of v(C=C), v(C=N) of tptz (*ca.* 1530 cm^{-1} as a strong singlet in free tptz) [17]. IR bands of **4–6** at 1614–1612 cm^{-1} and 1541–1532 cm^{-1} have been assigned to asymmetric (v_{as}) and symmetric (v_s) stretches of carboxyl group, respectively, indicating that coordination behavior of the benzoate groups is the same in all these complexes, i.e. bidentate. The position of IR bands at 1599 cm^{-1} (v_{as}) and 1421 cm^{-1} (v_s) are slightly different from bidentate benzoates. This coordination mode of carboxylate groups was further confirmed by X-ray crystallographic studies.

3.2. Description of crystal structures

3.2.1. Molecular structure of 1. This complex crystallizes in a orthorhombic system with space group *Pbcn* ($Z = 8$). The molecular structure of **1** is shown in figure 1, where the gadolinium center coordinates with N1, N2, and N3 from one tridentate tptz, N4, N5, and N6 from three thiocyanates, O1 from one water and O2 and O3 from two coordinated methanols. One uncoordinated methanol is also present in the lattice. The coordination polyhedron around Gd^{+3} is a slightly distorted tricapped trigonal prism (figure S1, see online supplemental material at http://dx.doi.org/10.1080/00958972.2014.992339). The Gd–N bond distances with tptz are 2.557(8)–2.605(8) Å, while with thiocyanates, 2.394(7)–2.464 (8) Å. The Gd–N bond distances with thiocyanates are shorter than that with tptz. The Gd–O bond distance is 2.426(6) Å with water, while 2.462(6)–2.481(7) Å with coordinated

Table 1.   Crystallographic data and structure refinement for **1–6**.

	Complex **1**	Complex **2**	Complex **3**	Complex **4**	Complex **5**	Complex **6**
Empirical formula	C$_{24}$H$_{22}$N$_9$O$_4$S$_3$Gd	C$_{24}$H$_{23}$N$_9$O$_4$S$_3$Eu	C$_{21}$H$_{12}$N$_9$O$_3$S$_3$ Tb	C$_{78}$H$_{54}$N$_{12}$O$_{16}$Gd$_2$	C$_{79}$H$_{58}$N$_{12}$O$_{22}$Eu$_2$	C$_{160}$H$_{122}$N$_{24}$O$_{32}$Tb$_4$
Formula weight	753.97	749.69	693.54	1729.83	1831.32	3528.54
T (K)	296(2)	296(2)	296(2)	296(2)	296(2)	296(2)
Crystal system	Orthorhombic	Orthorhombic	Triclinic	Monoclinic	Triclinic	Triclinic
Space group	*P b c n*	*P b c n*	*P-1*	*P 21/c*	*P 1*	*P-1*
Unit dimensions						
a (Å)	27.024(12)	27.124(3)	14.055(9)	13.275(17)	12.927(11)	14.253(11)
b (Å)	14.987(7)	15.117(2)	20.821(15)	15.035(17)	12.930(10)	15.754(13)
c (Å)	14.156(6)	14.291(2)	20.825(15)	18.810(2)	13.791(11)	17.686(17)
α (°)	90.00	90.00	83.66(6)	90.00	82.62(5)	67.53(3)
β (°)	90.00	90.00	70.28(3)	95.91(6)	83.15(4)	88.23(3)
γ (°)	90.00	90.00	70.33(4)	90.00	64.85(4)	82.09(3)
Volume (Å³)	5733(4)	5859.8(13)	5402.8(7)	3734.6(8)	2064.2(3)	3634.4(5)
Z	8	8	8	2	1	1
D$_{Calcd}$ (g cm^{-3})	1.747	1.700	1.705	1.538	1.473	1.612
μ (Mo K$_α$) (mm^{-1})	2.580	2.402	2.890	1.836	1.584	2.009
Crystal size (mm)	0.29 × 0.23 × 0.15	0.27 × 0.21 × 0.17	0.33 × 0.27 × 0.22	0.27 × 0.13 × 0.17	0.29 × 0.21 × 0.14	0.33 × 0.23 × 0.19
θ$_{max}$ (°)	28.47	31.64	28.51	28.56	28.47	27.51
Reflections measured	6755	8332	25,777	9285	16,186	15,839
Observed reflections	4118	6807	7753	6356	10,729	11,718
Data/restraints/parameters	6755/131/374	8332/0/378	25,777/0/1333	9285/0/487	16,186/0/1038	15,839/0/994
Final R indices [*I* > 2(*I*)]						
^{a}R$_1$	0.0642	0.0416	0.0774	0.0361	0.0667	0.0434
^{b}wR$_2$	0.1583	0.1549	0.1661	0.1028	0.1538	0.1214
CCDC no.	1004124	1004122	1004126	1004125	1004121	1004123

$^a R_1 = \sum \left| \left| F_o \right| - \left| F_c \right| \right| / \sum \left| F_o \right|$.
$^b wR_2 = \{ \sum [w (F_o{}^2 - F_c{}^2)^2] / \sum w (F_o{}^2)^2 \}$.

Table 2. Noncovalent interactions (Å and °) for **1–6**.

S. no.	D–H···A	d(D–H)	d(H–A)	d(D–A)	⟨(DHA)⟩
1.	**Complex 1**				
	O4–H4···S1	0.820	2.518(4)	3.335	174.9
	C4–H4A···O1	0.930	2.503(7)	3.379	157.1
	C10–H10···O4	0.932	2.601(11)	3.406	144.9
	C4–H4A···π	0.930	3.675(1)	3.470	170.1
	C10–H10A···π	0.932	3.514(1)	3.411	176.0
2.	**Complex 2**				
	O1–H1A···S2	0.829	2.475(56)	3.289	167.4
	O4–H4···S3	0.820	2.535(1)	3.355	177.4
	C19–H19···S1	0.931	3.176(1)	4.091	167.8
	C20–H20···S3	0.931	3.083(2)	3.721	127.3
	C26–H26B···S3	0.961	2.967(2)	3.662	130.2
3.	**Complex 3**				
	C46–H46···π	0.932	3.563(3)	3.591	184.2
	C60–H60···π	0.929	3.253(1)	3.433	193.2
4.	**Complex 4**				
	C3–H3···O2	0.930	2.573(6)	3.208	125.8
	C4–H4···O2	0.930	2.691(3)	3.262	120.3
	C4–H4···O4	0.930	2.838(7)	3.484	127.5
	C10–H10···O8	0.930	2.991(24)	3.875	159.4
	C23–H23···O8	0.930	2.961(22)	3.560	123.5
	C35–H35···O7	0.931	2.537(7)	3.338	144.4
5.	**Complex 5**				
	C82–H82A···O20	0.959	1.887(3)	2.845	177.6
	C82–H82B···O21	0.957	2.121(22)	2.755	122.3
	C82–H82C···O21	0.960	2.637(24)	2.755	86.7
	C19–H19···π	0.925	3.477(6)	3.821	113.6
	C20–H20···π	0.932	3.627(6)	3.687	121.5
	C37–H37···π	0.936	3.548(12)	3.699	91.86
	C52–H52···π	0.931	3.553(11)	3.651	88.6
6.	**Complex 6**				
	C80–H80B···O10	0.960	1.928(5)	2.866	164.9
	C3–H3···π	0.930	3.409(3)	4.018	125.1
	C11–H11···π	0.930	3.371(6)	4.165	144.6
	C12–H12···π	0.930	3.279(7)	3.742	112.9
	C13–H13···π	0.930	3.148(5)	3.674	117.7
	C23–H23···π	0.931	3.389(5)	3.464	74.34
	C36–H36···π	0.929	3.194(5)	3.753	120.5
	C46–H46···π	0.930	3.401(6)	4.262	154.9
	C60–H60···π	0.930	3.587(7)	4.468	159.0

methanol. Single-crystal X-ray study reveals that uncoordinated methanol is hydrogen bonded to coordinated thiocyanate where the methanolic oxygen is a hydrogen donor [O4–H4···S1, 2.518(4) Å]. The methanolic O4 also is a hydrogen acceptor with tptz ligand [C10–H10···O4, 2.601(11) Å] (figure S2a). Two neighboring mononuclear complexes are interconnected via C–H···O and C–H···π interactions [(i) C4–H4A···O1, 2.503(7) Å; (ii) C4–H4···π, 3.675(1) Å; (iii) C10–H10···π, 3.514(1) Å] (figure S2b). Other weak noncovalent interactions [O3···S2, 3.258(6) Å; S1···S1, 3.155(5) Å] are due to coordinated methanol and thiocyanate in adjacent complexes (figure S2c). All these intermolecular interactions construct a 3-D pseudo host–guest supramolecular motif along the 'c' axis, where the methanol is a guest (figure 2).
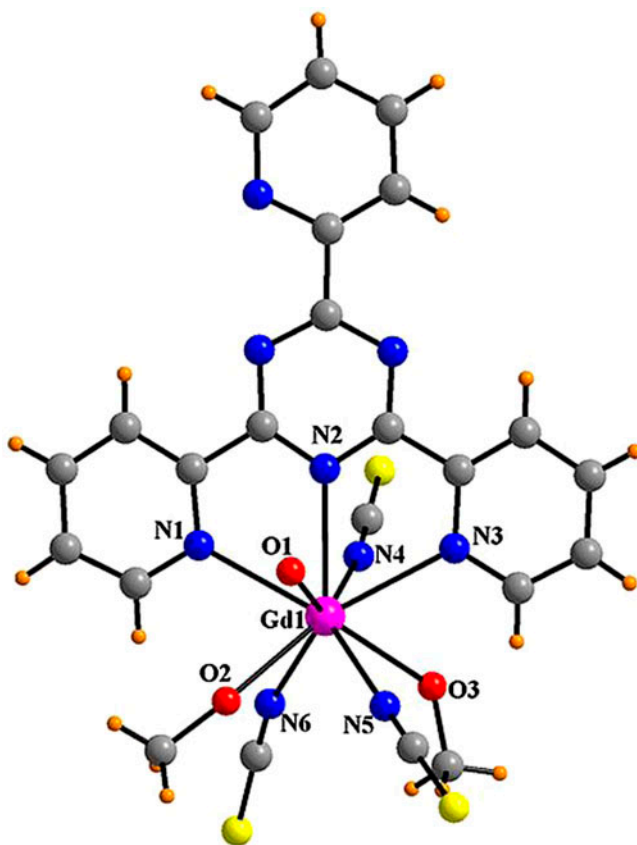
Figure 1. Molecular structure of **1** (CH₃OH is omitted for clarity). Color code: C, gray; H, orange; O, red; N, blue; S, yellow; Gd, purple (see http://dx.doi.org/10.1080/00958972.2014.992339 for color version).
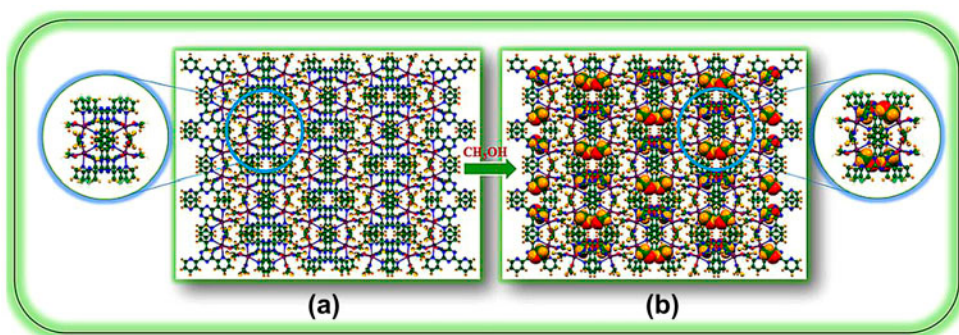

Figure 2. Pseudo host–guest supramolecular motif along the '*c*' axis in **1** (a) without guest (CH₃OH) and (b) with guest. Color code: C, green; H, orange; O, red; N, blue; S, yellow; Gd, purple (see http://dx.doi.org/10.1080/00958972.2014.992339 for color version).

3.2.2. Molecular structure of 2. This complex is isostructural with **1**, having the same geometry (figures 3 and S3). The Eu–N bond distances with tptz are 2.588(3)–2.636(5) Å, while with thiocyanates 2.434(4)–2.470(4) Å. Eu–N bond distances are larger than Gd–N in **1**. The Eu–O bond distances with methanol and water are 2.458(3)–2.517(4) Å, also greater than Gd–O bond distances in **1**. The uncoordinated methanol has intermolecular hydrogen bond interaction with the mononuclear europium complex, where O4 and methyl of methanol are donors with thiocyanates [O4–H4···S3, 2.535(1) Å, C26–H26B···S3, 2.967(2) Å]. The other hydrogen bonded intermolecular interactions [O1–H1A···S2, 2.475(56) Å; C19–H19···S1, 3.176(1) Å; C20–H20···S3, 3.083(2) Å] and very weak noncovalent interactions [O2···S1, 3.189(4) Å, S3···S3, 3.176(2) Å] are shown in figure S4. There are no C–H···π interactions in this complex as in **1**. These different noncovalent interactions construct a 3-D, ladder-like pseudo host–guest supramolecular arrangement along the '*b*' axis, where methanol in the lattice is a guest molecule (figure 4).
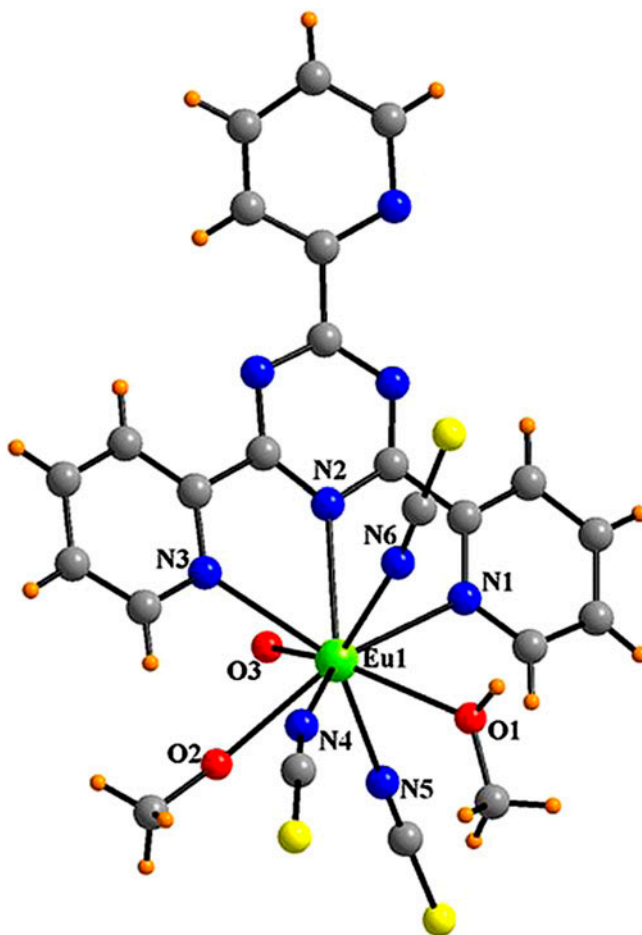

Figure 3. Molecular structure of **2** (CH$_3$OH is omitted for clarity). Color code: C, gray; H, orange; O, red; N, blue; S, yellow; Eu, green (see http://dx.doi.org/10.1080/00958972.2014.992339 for color version).

3.2.3. Molecular structure of 3. Single-crystal X-ray study predicts that **3** crystallizes in the triclinic system with space group *P-1* (*Z* = 8). The asymmetric unit consists of four molecules of mononuclear complex and all have the same structural dimensions and geometry. Each terbium center coordinates with N1, N2, and N3 of one tridentate tptz, N4, N5, and N6 of thiocyanates, and O1, O2, and O3 of water as shown in figure 5. The coordination polyhedron around each Tb^{+3} is a slightly distorted tricapped trigonal prism (figure S5). The Tb–N bond distances with tptz are 2.532(12)–2.620(12) Å, while with thiocyanates, they are 2.417(15)–2.497(15) Å. The Tb–O bond distances with water are 2.457(10)–2.536 (11) Å. The Tb–N and Tb–O bond distances are greater than that in **1** and **2**. As shown in figure S6, C–H⋯π [C46–H46⋯π, 3.563(3) Å; C60–H60⋯π, 3.253(1) Å] noncovalent interactions connect adjacent mononuclear complexes. Crystal packing also shows that one mononuclear complex is connected with six adjacent mononuclear units through very weak interactions [O3⋯S12, 3.395(13) Å; O4⋯S2, 3.195(15) Å; O6⋯S11, 3.166(13) Å; O7⋯S12, 3.295(17) Å; O8⋯S2, 3.188(14) Å; O9⋯S11, 3.186(15) Å; O10⋯S7, 3.309 (17) Å; O11⋯S9, 3.199(15) Å; O2⋯N27, 2.808(18) Å; S3⋯S8, 3.505(13) Å] (figure S7). A 3-D Mat like perspective view along the '*c*' axis is formed due to these noncovalent interactions (figure 6).

3.2.4. Molecular structure of 4. Single-crystal X-ray diffraction studies confirm the formulation of **4** as [Gd(tptz)(OBz)₂(μ-OBz)OH₂]₂·2H₂O. It crystallizes in the monoclinic space group *P 21/c* (*Z* = 2) and contains a binuclear metal center in which each gadolinium is coordinated by N1, N2, and N3 from a tptz, O1, O2, O3, O4, and O6 from four benzoates, and O5 from coordinated water, having coordination number nine as shown in figure 7. Two water molecules are present in the lattice. The coordination polyhedron around Gd^{+3} is a slightly distorted tricapped trigonal prism (figure S8). The gadoliniums are separated by 4.763(11) Å. Structural studies of lanthanide carboxylate complexes have shown that carboxylate groups may be coordinated simultaneously in three modes: chelating, bridging and
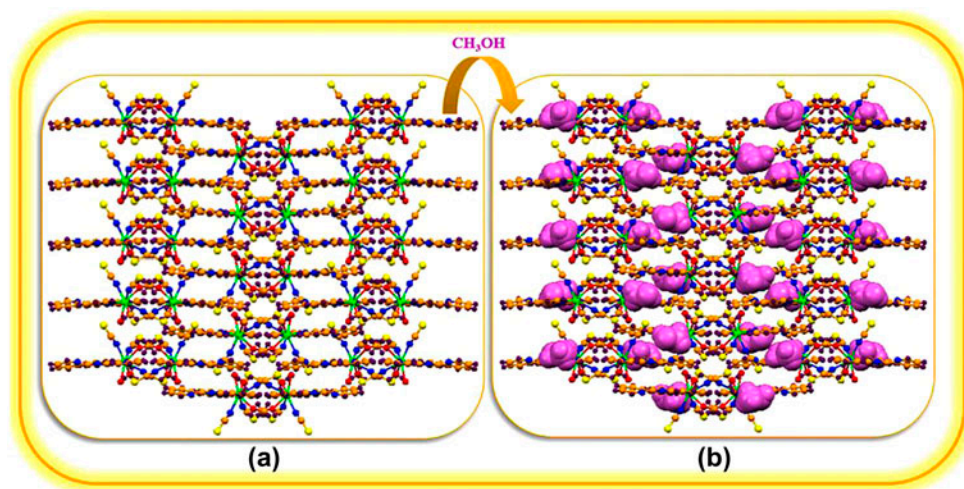

Figure 4.   Ladder-like pseudo host–guest supramolecular arrangement along the '*b*' axis in **2** (a) without guest (CH₃OH) and (b) with guest. Color code: C, orange; H, purple; O, red; N, blue; S, yellow; Eu, green; lattice CH₃OH, violet (see http://dx.doi.org/10.1080/00958972.2014.992339 for color version).
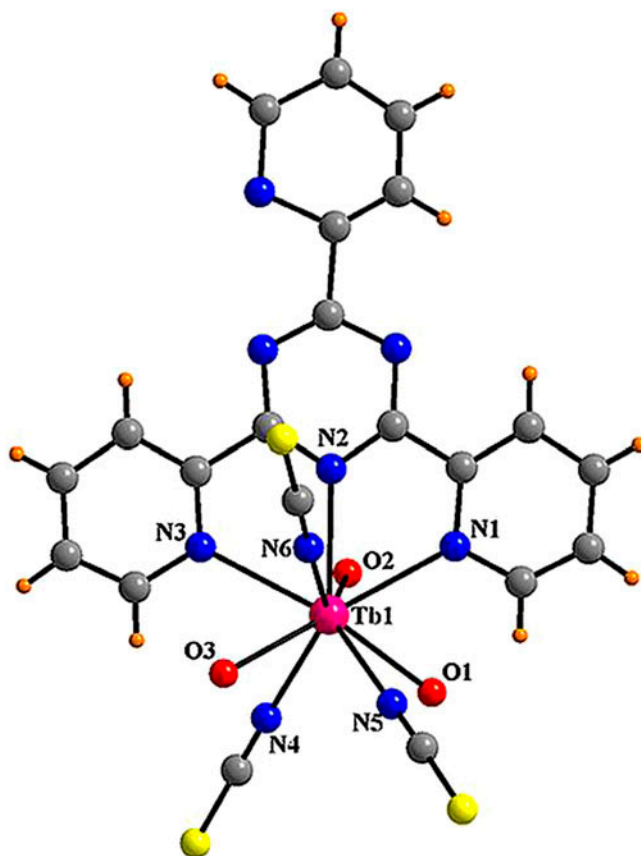
Figure 5.   Molecular structure of **3**. Color code: C, gray; H, orange; O, red; N, blue; S, yellow; Tb, pink (see http://dx.doi.org/10.1080/00958972.2014.992339 for color version).

chelating bridging [35, 36]. In the present structure, X-ray studies show that all four benzo-ates are coordinated in chelate-bridge mode within the dimeric unit, i.e. one benzoate is monodentate, while the other is bidentate. The other two benzoates bridge metals as can be seen from the differences in bond distances of Gd–O for coordinated benzoate (table S1). The Gd–O bond distances with benzoates are 2.307(4)–2.513(4) Å, and bridged benzoates have shorter distance when compared with other coordinated benzoates. The Gd–N bond distances with tptz are 2.617(11)–2.627(6) Å. According to figure S9, the uncoordinated water molecules hydrogen bond to the coordinated benzoates and tptz via C10–H10···O8, 2.991 (27) Å; C23–H23···O8, 2.961(27) Å interactions where it acts as an acceptor, while C–H···O interactions between adjacent complexes are C3–H3···O2, 2.573(6) Å; C4–H4···O2, 2.691 (3) Å; C4–H4···O4, 2.838(7) Å; C35–H35···O7, 2.537(7) Å. A spiral-like sheet along the '*a*' axis is possible due to these intermolecular hydrogen bond interactions (figure 8).

3.2.5. Molecular structure of 5. This complex crystallizes in the triclinic system with space group *P 1* (*Z* = 1). Each metal center completes its coordination number (nine) through three nitrogens from tridentate tptz ligands, five oxygens from benzoates, and one oxygen
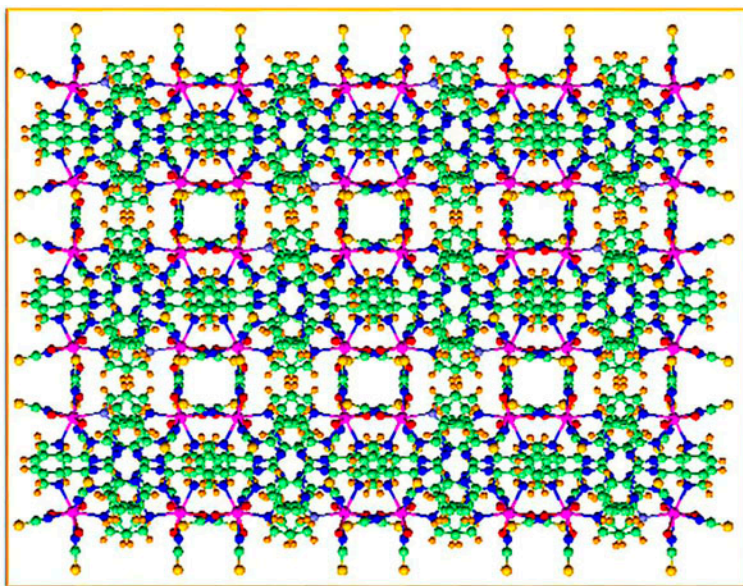
Figure 6. Mat-like perspective view along the '*c*' axis in **3**. Color code: C, green; H, orange; O, red; N, blue; S, yellow; Tb, pink (see http://dx.doi.org/10.1080/00958972.2014.992339 for color version).
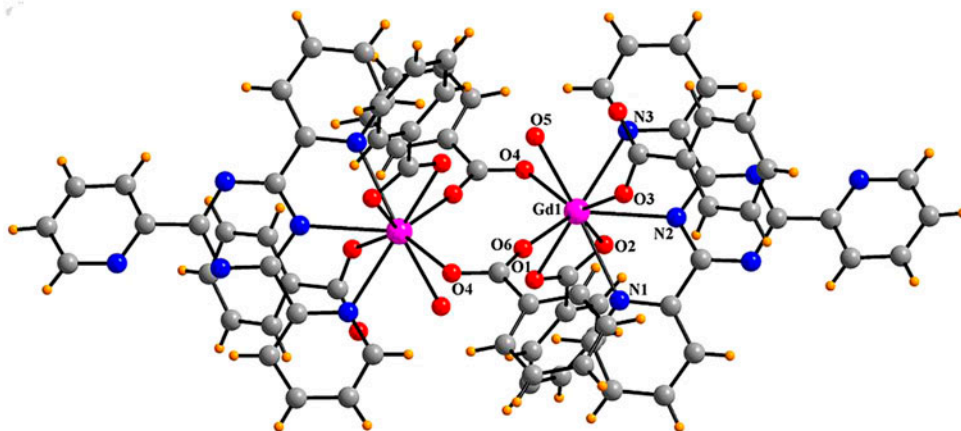

Figure 7. Molecular structure of **4** (H_2O are omitted for clarity). Color code: C, gray; H, orange; O, red; N, blue; Gd, purple (see http://dx.doi.org/10.1080/00958972.2014.992339 for color version).

from water (figure 9). Seven waters and one methanol are present in the lattice. The coordination polyhedron of Eu^{+3} is a slightly distorted tricapped trigonal prism (figure S10). The Eu–N bond distances with tptz are 2.583(23)–2.660(29) Å, while the Eu–O bond distances with benzoates are 2.236(19)–2.524(19) Å. The bridged benzoates have shorter distance when compared with terminally coordinated benzoates. The binuclear europium complex is hydrogen bonded to the neighboring complex via C–H···π [C19–H19···π, 3.477(6) Å;
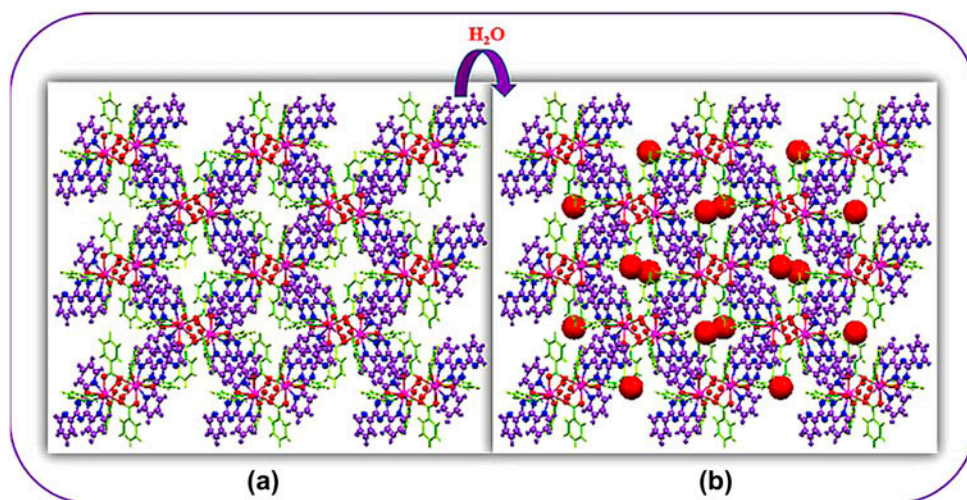
Figure 8. Spiral-like sheet along the '*a*' axis in **4** (a) without and (b) with H_2O molecules. Color code: O, red; N, blue; Gd, purple; tptz, violet; Bz, green; lattice H_2O, red (see http://dx.doi.org/10.1080/00958972.2014.992339 for color version).

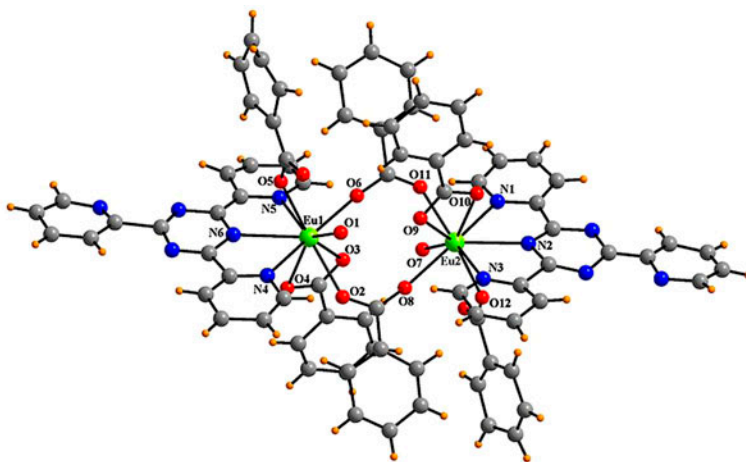
Figure 9. Molecular structure of **5** (CH_3OH and H_2O omitted for clarity). Color code: C, gray; H, orange; O, red; N, blue; Eu, green (see http://dx.doi.org/10.1080/00958972.2014.992339 for color version).

C20–H20···π, 3.627(6) Å; C37–H37···π, 3.548(12) Å; C52–H52···π, 3.553(11) Å] intermolecular interactions. Due to these C–H···π interactions, four binuclear complexes hydrogen bond to each other and construct a cavity for guest molecules, i.e. behave as a host. The seven waters and one methanol are guest molecules and occupy these cavities. The seven water molecules bond to each other via O···O [O17···O19, 2.997(35) Å; O19···O20, 2.787(31) Å; O17···O22, 3.008(31) Å; O15···O16, 2.737(39) Å; O15···O22, 2.690(47) Å; O16···O21, 2.886(40) Å] intermolecular interactions. Three uncoordinated water molecules show intermolecular interactions with the coordinated benzoates through O···O [O4···O20, 2.703(29)
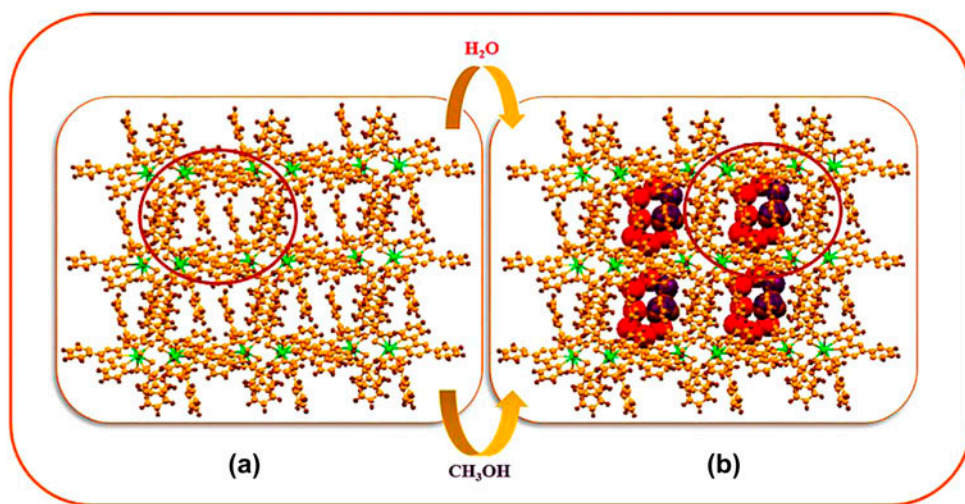
Figure 10. Host–guest supramolecular framework along the '*a*' axis in **5** (a) without guest (H$_2$O, CH$_3$OH) and (b) with guest. Color code: C, O, N, orange; H, brown; Eu, green; lattice H$_2$O, red; lattice CH$_3$OH, purple (see http://dx.doi.org/10.1080/00958972.2014.992339 for color version).

Å; O13···O17, 2.892(31) Å; O10···O15, 2.851(32) Å; O14···O21, 2.878(36) Å] weak inter-actions. The methanol is also involved in noncovalent interactions [C82–H82A···O20, 2.845 (36) Å; C82–H82B···O21, 2.121(22) Å; C82–H82C···O21, 2.637(24) Å] with uncoordi-nated water, where the methyl is a donor and water an acceptor (figure S11). All of these interactions help to construct an entirely different 3-D, host–guest supramolecular framework along the '*a*' axis for this complex (figure 10).

3.2.6. Molecular structure of 6. The unit cell consists of two crystallographically inde-pendent complexes, two mononuclear, and one binuclear complex with four waters and two methanols in the lattice (figure 11). This complex crystallizes in a triclinic system with space group *P-1* (*Z* = 1). In the binuclear complex, each metal center (Tb1) is coordinated by N1, N2, and N3 from tptz and O1, O2, O3, O4, O5, and O6 from benzoates (two OBz are bidentate and two bridging). In the mononuclear unit, Tb2 is nine coordinate by N, N8, and N9 from tptz, O7, O8, O9, O10, and O11 from three benzoates (two OBz are bidentate and one monodentate). The coordination polyhedron is completed by one methanol. A coor-dinated polyhedron around each Tb^{+3} is a slightly distorted tricapped trigonal prism (figure S12). The Tb–N bond distances in the binuclear unit are 2.566(6)–2.601(6) Å and the Tb–O distances are 2.265(6)–2.485(6) Å, while the Tb–N bond distances in the mononu-clear unit are 2.524(6)–2.569(6) Å and the Tb–O distances are 2.377(7)–2.487(5) Å. The Tb–N bond distances in the binuclear complex are greater and Tb–O distances are lesser than that in the mononuclear complex. Different C–H···π interactions are present in this complex: (i) binuclear moiety noncovalently hydrogen bonded to adjacent binuclear com-plexes through C12–H12···π, 3.148(5) Å; C13–H13···π, 3.279(7) Å; C23–H23···π, 3.389 (5) Å, (ii) two mononuclear complexes are hydrogen bonded via C3–H3···π, 3.409(3) Å, (iii) mononuclear and binuclear complexes are hydrogen bonded to each other via C3–H3···π, 3.409(3) Å; C11–H11···π, 3.371(6) Å which are involved in making a cavity to
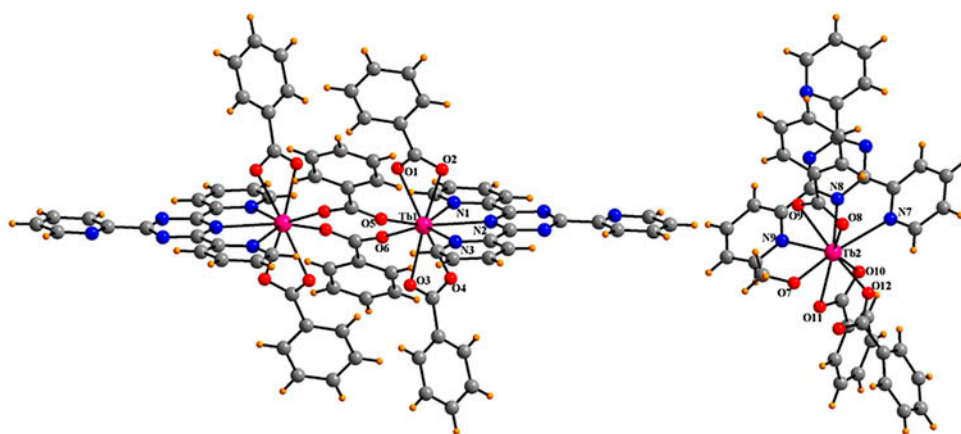
Figure 11. Molecular structure of **6** (CH_3OH and H_2O omitted for clarity). Color code: C, gray; H, orange; O, red; N, blue; Tb, pink (see http://dx.doi.org/10.1080/00958972.2014.992339 for color version).

occupy the methanol and water molecules. The methanol occupied the cavity through C80–H80B⋯O10, 1.928(5) Å, while the water molecules interact with oxygens of benzoates and nitrogen of tptz via O1⋯O15, 2.738(8) Å; O2⋯O14, 2.847(8) Å; O3⋯O15, 2.761(7) Å; N6⋯O14, 2.985(8) Å intermolecular interactions, respectively (figure S13). The intermolecular interactions are responsible for formation of an entirely different 3-D supramolecular motif along the '*b*' axis as shown in figure 12.

3.3. *Photophysical properties*

Due to electronic arrangement in inner *f* orbitals of metal ions, lanthanide complexes show high luminescence efficiency with characteristic sharp bands, and luminescence efficiency
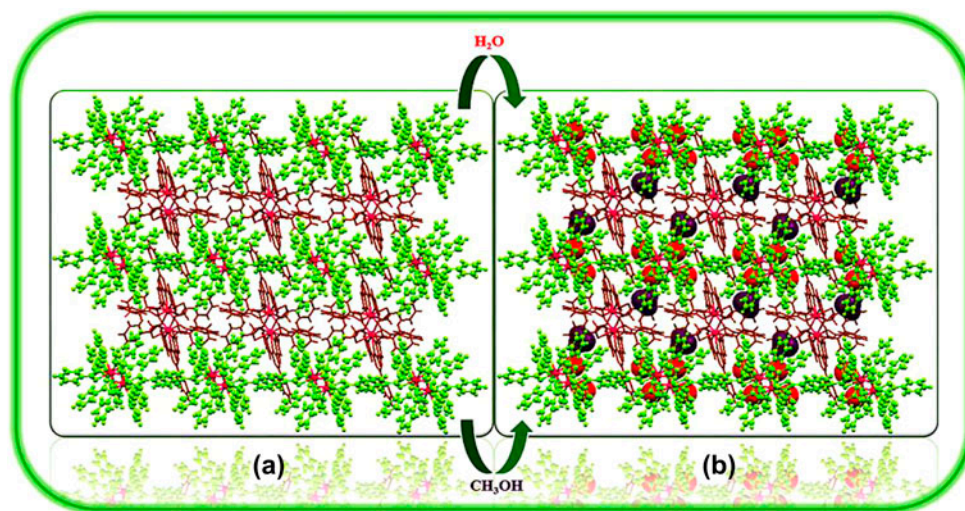

Figure 12. 3-D supramolecular motif along the '*b*' axis in **6** (a) without and (b) with H_2O, CH_3OH molecules. Color code: Tb, pink; binuclear unit, green; mononuclear unit, brown; lattice H_2O, red; lattice CH_3OH, purple (see http://dx.doi.org/10.1080/00958972.2014.992339 for color version).

increases as the chelation increases in complexes [37]. No emission could be detected for the Gd complexes. The ultraviolet absorption spectra (spectra not shown) of **2** shows maximum absorption bands at 292.0 nm, while the emission spectrum displays bands at 585.6 nm ($^5D_0 \rightarrow {}^7F_1$), 618.0 nm ($^5D_0 \rightarrow {}^7F_2$), 648.4 nm ($^5D_0 \rightarrow {}^7F_3$), and 691.6 nm ($^5D_0 \rightarrow {}^7F_4$) as shown in figure 13(a). The electronic dipole transition $^5D_0 \rightarrow {}^7F_1$ exhibits the highest relative emission intensity. From the spectrum, it is clear that very efficient energy transfer occurs from the ligands to Eu(III), i.e. no emission from the ligands. UV–vis absorption spectra of **5** reveals absorption bands at λ_{max} = 230 nm. Complex **5** shows more emission bands with greater number of transitions ($^5D_0 \rightarrow {}^7F_{0, 1, 2, 3, 4}$) and 616.1 nm ($^5D_0 \rightarrow {}^7F_2$) show the highest relative emission intensity [figure 13(b)]. The $^5D_0 \rightarrow {}^7F_0$ shows an asymmetrical and relatively weak transition. The inhomogeneous broadening of the $^5D_0 \rightarrow {}^7F_0$ emission band arises from site to site variation in the local field acting on the ions. The emission spectrum of **5** is quite different from **2** as the crystal system is
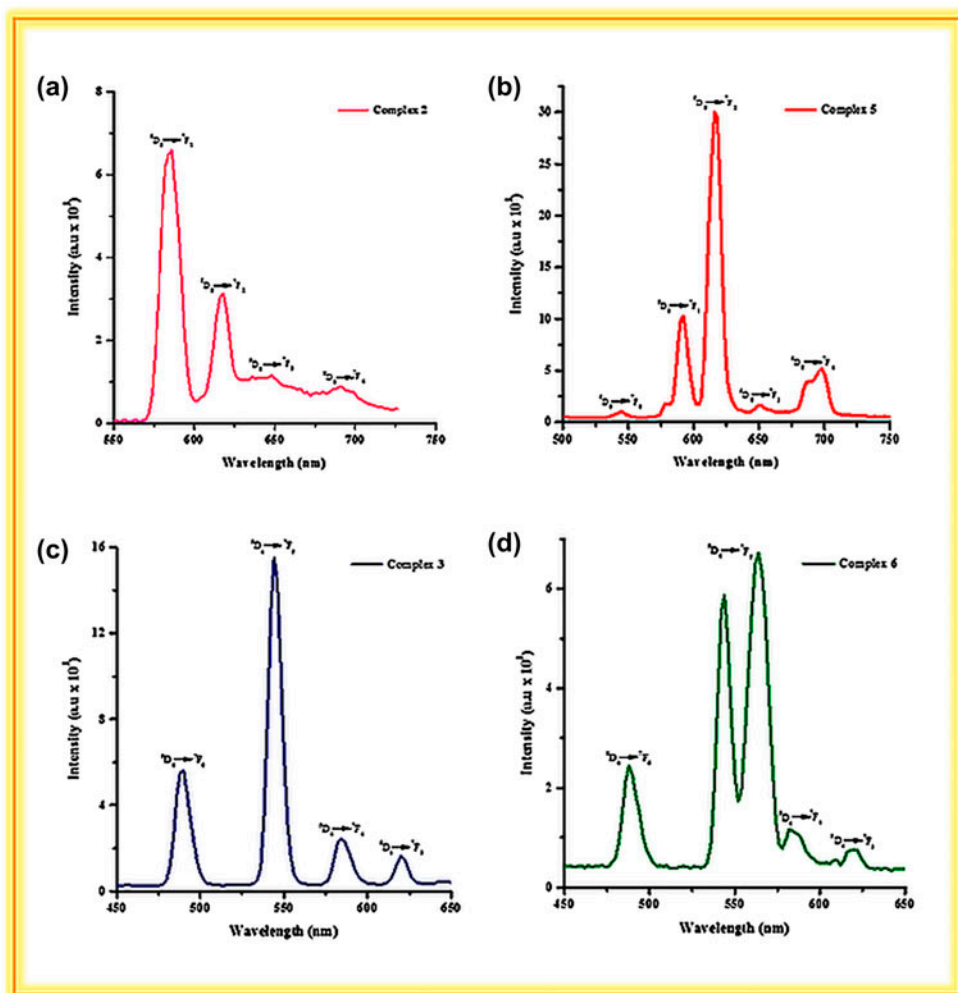

Figure 13.   Emission spectra of **2**, **3**, **5** and **6**.

triclinic, and the benzoate groups chelate, whereas **2** is mononuclear, and crystallizes in the orthorhombic crystal system. In **3**, the emission spectrum of Tb (λ_{max} = 264 nm) exhibits typical narrow bands, which arise from $^5D_4$ ground state to the ^7F_j (J = 6–0) multiplet transition. The bands at 489.0, 544.4, 581.6, and 622.0 nm are attributed to the transition from $^5D_4$ state to $^7F_6$, $^7F_5$, $^7F_4$, and $^7F_3$, respectively [figure 13(c)]. The most intense band is observed at 544.4 nm, due to $^5D_4 \rightarrow {}^7F_5$ transition. According to figure 13(d), the emission spectrum of **6** exhibits specific maxima at 489.0, 544.8, 565.0, 587.1, and 621.7 nm. The number of components of the $^5D_4 \rightarrow {}^7F_5$ transition indicates the presence of more than one chemically different Tb(III) site. This is the most intense peak. Complexes **3** and **6** have different spectra as **3** is mononuclear, whereas **6** contains both binuclear and mononuclear units with different local coordination. Thus, the coordination environment around Ln(III) changes the fluorescence spectra, i.e. the emission spectra are very sensitive to the structural changes as also suggested by Legendziewicz *et al.* [38, 39].

3.4. *Thermal study*

The thermograms are recorded for all the complexes by TG and DTG technique from 20 to 800 °C at a heating rate of 10 °C min^{-1} in air. TG analysis indicates the complexes are stable at room temperature but at higher temperatures, curves show irregular pattern until plateau is reached at 800 °C due to the formation of thermally stable lanthanide oxides (Ln_2O_3) [40]. The thermoanalytical data for **1–6** are listed in table 3. According to TG curve as shown in figure 14, **1** and **2** show the same pattern of thermal decomposition with two well-separated weight loss stages. In the first step of **1**, one uncoordinated methanol with 4.1% mass loss leaves at 117–176 °C, while in **2** it releases with ~4.09% mass loss at 131–174 °C and corresponds to DTG peak at 169 °C. In the second stage, one 2,4,6-tris(2-pyridyl)-1,3,5-triazine, three thiocyanates, two methanols, and one water are released with ~74.3 and ~74.7% weight loss from 263 to 513 °C and 255 to 516 °C (DTG peaks at 471 °C and 381 °C) for **1** and **2**, respectively. Complex **3** undergoes one step decomposition. This step (76.7% mass loss) corresponds to DTG peak at 423 °C. In this step, one 2,4,6-tris(2-pyridyl)-1,3,5-triazine, three thiocyanates, and three water molecules (271–532 °C) are lost. Thermal decomposition of **4** can be divided into two stages. The first weight loss of 2.0% between 134 and 188 °C (DTG peak at 161 °C) predicts the release of uncoordinated water. The second weight loss, 78.6%, is observed from 231 to 568 °C that corresponds to DTG peak at 293 °C. The water in the lattice is less stable, easily removed

Table 3.   TG-DTG data of **1–6**.

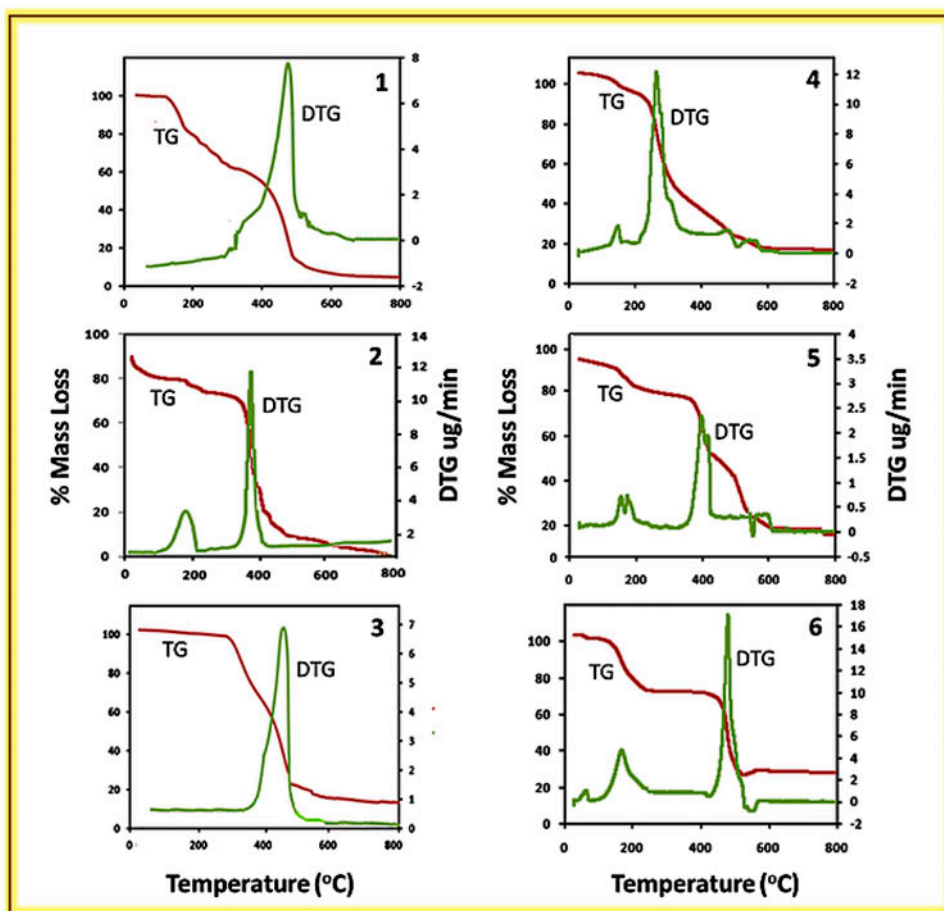| S. no.	Complexes	T_i/(°C)	TG T_f/(°C)	α	DTG Peak temp./(°C)
1.	Complex **1**	117	176	4.1	–
		263	513	74.3	471
2.	Complex **2**	131	174	4.09	169
		255	516	74.7	381
3.	Complex **3**	271	532	76.7	423
4.	Complex **4**	134	188	2.0	161
		231	567	78.6	293
5.	Complex **5**	139	177	8.2	167
		327	581	73.8	409
6.	Complex **6**	94	113	3.4	97
		173	287	38.7	187
		401	579	46.6	497

Figure 14.   Simultaneous TG-DTG of **1–6** in air.

in comparison to coordinated molecules. Complex **5** shows the same thermal decomposition pattern as **4** but in **5**, one methanol and seven water molecules are released at 167 °C DTG peak with 8.2% weight loss at 139–177 °C in the first step, while 73.8% weight loss between 327 and 581 °C at 409 °C DTG peak in next second step is due to the remaining coordinated groups. The TG thermogram clearly indicates that thermal decomposition of **6** occurs in three steps. This complex on heating first loses 2.5% of its mass at 94–113 °C from loss of methanol and water in the lattice. Beyond this temperature, a plateau is observed where 38.7% mass loss occurs from removal of $C_{40}H_{31}N_6O_7$ at 173–287 °C with DTG peak at 187 °C. Almost complete decomposition (46.6%) occurs at 579 °C (DTG peak at 497 °C), which corresponds to release of $C_{78}H_{54}N_{12}O_{12}$.

4. Conclusion

We report the synthesis, structures, photophysical, and thermal properties of mononuclear and binuclear lanthanide complexes using tptz and benzoate ligands. All lanthanide

complexes show nine-coordination depending on the presence of different types of ligands in the reaction mixture. Complexes **1–3** with tptz give the mononuclear unit, while in the presence of benzoate in the reaction mixture, **4–6** give the 3-D bridging architecture. Complex **6** possesses two types of chemical environments for Tb^{+3} ions in the crystal. The structural integrity and the highly ordered arrangement of lanthanide centers in these complexes provide applications as structural and functional building blocks for a variety of lanthanide-containing materials. The photophysical properties of these have been studied with excitation and emission spectra, and reveal the presence of a single luminescent site, i.e. efficient ligand-to-metal energy transfer. Thermal analysis shows that all synthesized complexes are stable at room temperature and decompose at high temperature to give stable lanthanide oxides.

Supplementary material

CCDC numbers 1004121–1004126 contain the supplementary crystallographic data (CIF) for this article. These data can be obtained free of charge from the Director, CCDC, 12 Union Road, Cambridge CB2 1EZ, UK (Fax: +44 1223 336 033; E-mail: deposit@ccdc.cam.ac.uk or http://www.ccdc.cam.ac.uk). Additional figures (figures S1–S13) and tables (tables S1 and S2) are available in PDF formats.

Acknowledgements

References

[1] M. Sun, H. Xin, K.Z. Wang, Y.A. Zhang, L.P. Jin, C.H. Huang. *Chem. Commun.*, **6**, 702 (2003).
[2] G.F. de Sá, O.L. Malta, C. de Mello Donegá, A.M. Simas, R.L. Longo, P.A. Santa-Cruz, E.F. da Silva Jr. *Coord. Chem. Rev.*, **196**, 165 (2000).
[3] G. Vicentini, L.B. Zinner, J. Zukerman-Schpector, K. Zinner. *Coord. Chem. Rev.*, **196**, 353 (2000).
[4] Y. Li, F.-K. Zheng, X. Liu, W.-Q. Zou, G.-C. Guo, C.-Z. Lu, J.-S. Huang. *Inorg. Chem.*, **45**, 6308 (2006).
[5] T. Jin, A. Tsutsumi, Y. Deguchi, K.I. Machida, G.Y. Adachi. *J. Electrochem. Soc.*, **142**, L195 (1995).
[6] T. Jin, S. Tsutsumi, Y. Deguchi, K.I. Machida, G.Y. Adachi. *J. Alloys Compd.*, **252**, 59 (1997).
[7] B. Yan, H.J. Zhang, J.Z. Ni. *Mater. Sci. Eng.*, **52**, 123 (1998).
[8] X.H. Chuai, H.J. Zhang, F.S. Li. *Mater. Lett.*, **46**, 244 (2000).
[9] B. Yan, Y.S. Song. *J. Fluoresc.*, **14**, 289 (2004).
[10] N. Sabbatini, M. Guardigli, I. Manet, R. Ungaro, A. Casnati, R. Ziessel, G. Ulrich, Z. Asfari, J.-M. Lehn. *Pure Appl. Chem.*, **67**, 135 (1995).
[11] G.F. de Sá, F.R.G. e Silva, O.L. Malta. *J. Alloys Compd.*, **207–208**, 457 (1994).
[12] O.A. Serra, I.L.V. Rosa, E.J. Nassar, P.S. Calefi, P.C. Cardoso. *J. Alloys Compd.*, **249**, 178 (1997).
[13] G. Ionova, C. Rabbe, R. Guillaumont, S. Ionov, C. Madic, J.-C. Krupa, D. Guillaneux. *New J. Chem.*, **26**, 234 (2002).
[14] M.G.B. Drew, M.J. Hudson, P.B. Iveson, C. Madic. *Acta Crystallogr., Sect. C*, **56**, 434 (2000).
[15] P. Paul, B. Tyagi, A.K. Bilakhiya. *Inorg. Chem.*, **37**, 5733 (1998).
[16] R. Zibaseresht, R.M. Hartshorn. *Aust. J. Chem.*, **58**, 345 (2005).
[17] L. Zhang, X.Q. Lu, Q. Zhang. *Trans. Met. Chem.*, **30**, 76 (2005).
[18] E. Niyama, H.F. Brito, M. Cremona, E.E.S. Teotonio, R. Reyes, G.E.S. Brito. *Spectrochim. Acta*, **61**, 2643 (2005).
[19] H.B. Xu, L.X. Shi, E. Ma, L.-Y. Zhang, Q.-H. Wei. *Chem. Commun.*, **38**, 1601 (2006).

[20] P. Coppo, M. Duati, V.N. Kozhevnikov, J.W. Hofstraat, L. De Cola. *Angew. Chem. Int. Ed.*, **44**, 1806 (2005).
[21] G.M. Davies, S.J.A. Pope, H. Adams, S. Faulkner, M.D. Ward. *Inorg. Chem.*, **44**, 4656 (2005).
[22] A. Bourdolle, M. Allali, J.-C. Mulatier, B. Le Guennic, J.M. Zwier, P.L. Baldeck, J.-C.G. Bünzli, C. Andraud, L. Lamarque, O. Maury. *Inorg. Chem.*, **50**, 4987 (2011).
[23] S. Swavey. *J. Chem. Educ.*, **87**, 727 (2010).
[24] Y. Gai, F. Jiang, L. Chen, M. Wu, K. Su, J. Pan, X. Wan, M. Hong. *Cryst. Growth Des.*, **14**, 1010 (2014).
[25] J.-H. Xue, X.-H. Hua, L.-M. Yang, W.-H. Li, Y.-Z. Xu, G.-Z. Zhao, G.-H. Zhang, K.-X. Liu, J.-E. Chen, J.-G. Wu. *Chin. Chem. Lett.*, **25**, 887 (2014).
[26] C.S. Stan, I. Rosca, D. Sutiman, M.S. Secula. *J. Rare Earths*, **30**, 401 (2012).
[27] R. Kumar, U.P. Singh. *J. Coord. Chem.*, **61**, 2663 (2008).
[28] G.M. Sheldrick. *SADABS*, University of Göttingen, Göttingen (1996).
[29] G.M. Sheldrick. *Acta Crystallogr.*, **46**, 467 (1990).
[30] G.M. Sheldrick. *SHELXTL-NT Version 6.12, Reference Manual*, University of Göttingen, Göttingen (2000).
[31] B. Klaus. *DIAMOND Version 1.2c*, University of Bonn, Bonn (1999).
[32] MERCURY. Cambridge Crystallographic Data Centre, Cambridge (1999). Available online at: http://www.ccdc.cam.ac.uk/
[33] K. Nakamoto. *Infrared Spectra of Inorganic and Coordination Compounds*, 3rd Edn, John Wiley, New York, NY (1986).
[34] R.M. Silverstein, G.C. Bassler, T.C. Morrill. *Spectrometric Identification of Organic Compounds*, 5th Edn, John Wiley, New York, NY (1991).
[35] N. Ren, J.-J. Zhang, R.-F. Wang, S.-P. Wang. *J. Chin. Chem. Soc.*, **53**, 293 (2006).
[36] N. Ren, J.-J. Zhang, S.-L. Xu, R.-F. Wang, S.-P. Wang. *Thermochim. Acta*, **438**, 172 (2006).
[37] W.D. Horrocks Jr., M. Albin. *Prog. Inorg. Chem.*, **31**, 1 (1984).
[38] T. Glowiak, J. Legendziewicz, E. Huskowska, P. Gawryszewska. *Polyhedron*, **15**, 2939 (1996).
[39] J. Legendziewicz, T. Głowiak, E. Huskowska, D. Cong Ngoan. *Polyhedron*, **7**, 2495 (1988).
[40] U.P. Singh, N. Goel, G. Singh, P. Srivastava. *Inorg. Chim. Acta*, **387**, 294 (2012).